PHYSICAL REVIEW B **87**, 064403 (2013)

Effect of Ba and Ti doping on magnetic properties of multiferroic $Pb(Fe_{1/2}Nb_{1/2})O_3$

V. V. Laguta,[1,2] M. D. Glinchuk,[2] M. Maryško,[1] R. O. Kuzian,[2] S. A. Prosandeev,[3,4] S. I. Raevskaya,[3] V. G. Smotrakov,[3] V. V. Eremkin,[3] and I. P. Raevski[3]

[1]*Institute of Physics AS CR, 16253 Prague, Czech Republic*

[2]*Institute for Problems of Materials Science, NASc of Ukraine, 03142 Kiev, Ukraine*

[3]*Department of Physics and Research Institute of Physics, Southern Federal University, 344090 Rostov on Don, Russia*

[4]*Department of Physics, University of Arkansas, Fayetteville, Arkansas 72701, USA*

(Received 22 November 2012; published 4 February 2013)

On the basis of extensive experimental studies of $Pb_{1-x}Ba_x(Fe_{1/2}Nb_{1/2})O_3$ (PFN-BFN) and $Pb(Fe_{1/2}Nb_{1/2})_{1-x}Ti_xO_3$ (PFN-PT) single crystals by several experimental methods, we have proposed phase diagrams describing the magnetic properties of these solid solutions. The comprehensive consideration of the magnetic properties of the PFN-based solid solutions has shown that these phase diagrams can be explained on the basis of a model suggested earlier for pure PFN [Phys. Rev. Lett. **105**, 257202 (2010)]. This model assumes the coexistence in the crystal lattice of the long-range antiferromagnetic (AFM) cluster, which defines the Néel order parameter, with the finite-size mixed ferromagnetic-AFM clusters, responsible for the spin-glass order parameter. We state that one of these parameters, the Néel temperature, linearly decreases with the increasing dopant concentration and eventually disappears at some critical concentration as a result of the percolation phase transition. The other parameter survives until the maximal concentrations studied. We have also found a phase which can be related to the super-AFM order. These data can have important implications and provide the basis for the development of novel fundamental theory of multiferroics with the site, charge, and spin disorder.

DOI: 10.1103/PhysRevB.87.064403 PACS number(s): 75.85.+t, 61.43.−j, 75.50.Lk, 77.80.Jk

I. INTRODUCTION

Double perovskite $Pb(Fe_{1/2}Nb_{1/2})O_3$ (PFN) has been the center of attention in recent years, because of its extreme multiferroic properties.[1–7] Interestingly, these properties can become even better[2,4,6–8] if one tunes them by means of doping (see, e.g., Refs. 6 and 7, and references therein). However, the microscopic origin of this influence is still unclear. We believe the answer to this nontrivial question lies in some specialties of the magnetic phase diagram of PFN-based solid solutions, which have been studied only scarcely.[4,6,7]

References 1–7 discuss the existence of the ferroelectric (FE), antiferromagnetic (AFM), and spin-glass (SG) phases in the PFN-based solid solutions and pure PFN. The SG phase[3] has been mostly studied in pure PFN. The μSR spectroscopy and neutron diffraction experiments[5] have shown that the magnetic ground state of PFN is of SG order, which coexists with the long-range AFM order, below $T_g \approx 20$ K. In a recent work, Kleemann *et al.*[3] suggested the occurrence in PFN below Néel temperature T_N of the superantiferromagnetic (SAF) clusters, which coexist with the long-range AFM phase (note that, originally, the concept of superantiferromagnetism was introduced by Néel, when interpreting the experimental results on the fine AFM particles[9]). Important results were also obtained by the nuclear magnetic resonance (NMR) and electron paramagnetic resonance (EPR) methods.[10–13] In particular, the ^{93}Nb NMR spectra in PFN[13] showed the coexistence of two different Nb sites which have different local magnetic fields originating from the Fe-rich (Nb-poor) and Fe-poor (Nb-rich) nanoregions. These data suggest that a SG state in PFN, below 20 K, might arise from the latter regions.[13]

The information about the PFN-based solid solutions is more restricted. Valuable data were obtained in Refs. 4 and 7 concerning the influence of the Ba and Ca substitution for Pb on the ferroelectric and magnetic properties of PFN, from the point of view of a possible leading role of the Pb ions in both the ferroelectric and magnetic coupling. In particular, the decrease of T_N with increase of the Ba doping was explained by possible involvement of the Pb ions in the superexchange of the iron ions. However, the ground magnetic state of the Ba-doped PFN remains unclear.

Similar problems also still exist for the Ti-doped solid solutions of PFN. References 6 and 7 contain the phase diagram of the magnetic and ferroelectric properties of Ti-doped PFN, built on the basis of the dielectric, pyroelectric, piezoelectric, Mossbauer, structural, and magnetization data, for a Ti concentration up to $x = 0.4$. In these phase diagrams, the ferroelectric-to-paraelectric phase transition temperature was shown to increase approximately linearly with x, while the temperature of the transition between the ferroelectric rhombohedral (monoclinic) and tetragonal phases decreases with x nonlinearly.[6,7] However, the magnetic characteristics still need further measurements and understanding.

The main aim of this paper is to report on experimental data about the magnetic properties of the Ti- and Ba-doped solid solutions of PFN, in order to utilize these data for plotting the concentration-temperature phase diagrams. We will show that these phase diagrams reveal fingerprint features of the percolation phase transitions of the AFM order in PFN on doping, which can help in the understanding of the changes of the properties of PFN with the concentration of the doping elements.

The plan of our paper is the following. After a short description of the list of the experimental methods in use (Sec. II), we report on our experimental exploration of the magnetic susceptibility (Sec. III A) and magnetization hysteresis loops (Sec. III B). Sec. III C presents our EPR data. Then, in Sec. IV, we discuss the results obtained.

Despite the existence of numerous studies of the magnetic properties of pure PFN,[1,2–7] we have repeated some of those measurements on our single crystal samples (the majority of the previous measurements were done on ceramics), and some measurements were totally original.

II. EXPERIMENT

Single crystals of $Pb_{1-x}Ba_x(Fe_{1/2}Nb_{1/2})O_3$ (PFN-BFN) at $x = 0$, 0.07, 0.17, 0.23, 0.3 and $Pb(Fe_{1/2}Nb_{1/2})_{1-x}Ti_xO_3$ (PFN-PT) at $x = 0$, 0.03, 0.12, 0.2 were grown by the spontaneous crystallization procedure from the PbO-B_2O_3 flux in the temperature range from 1010 °C to 850 °C (see details of this growing process in Ref. 14). The resulting crystals were cubic shaped, with the edges up to 4–6 mm and faces parallel to the (100) planes of the prototype perovskite structure. Chemical composition of the crystals was determined with the help of the electron probe x-ray microanalyzer "Camebax-Micro," using PFN, $PbTiO_3$, and $BaTiO_3$ single crystals as reference samples.

The BFN ceramics was prepared by the solid state reaction route as described in Ref. 4. The phase purity of all the compositions obtained was checked by x-ray diffraction, which showed a single phase of the perovskite type.

The magnetic measurements were carried out using the superconducting quantum interference device magnetometers MPMS-5S and MPMS-XL (Quantum Design). The magnetic susceptibilities were measured under the zero-field-cooled (ZFC) and field-cooled (FC) protocols, in the temperature range between 2 and 400 K. Additionally, the ac magnetic susceptibility was measured in the (0.12–262) Hz interval by employing the driving magnetic field of $H = 3.9$ Oe. We also recorded the magnetic hysteresis loop, at $T = 5$ K, in the interval of the magnetic field from -50 to 50 kOe. Subsequently, we measured the temperature dependence of the remanent magnetization, in the temperature interval from 4 to 50 K. All the measurements were carried out on samples which were not specifically oriented.

The main measurement, in this study, was done with the help of EPR spectroscopy. These measurements were performed at 9.25–9.8 GHz with a Bruker E580 spectrometer and Oxford Instrument cryostat, in the temperature range from 4 to 300 K. Note that EPR spectroscopy is capable of getting unique information about the phase diagrams of the solid solutions studied, because it is much more sensitive to the change of the magnetic state of local Fe^{3+} magnetic moments than the magnetic susceptibility measurements.

III. EXPERIMENTAL DATA

A. Magnetic susceptibility studies

The results of the measurements of the ZFC and FC magnetic susceptibility for pure PFN are presented in Fig. 1 [panel (a)]. One can see that the ZFC magnetic susceptibility $\chi_{ZFC}(T)$ exhibits a pronounced maximum, in the low-temperature region. In accord with Ref. 3, we found the position of this maximum dependent on the magnetic field H. Besides the low-temperature maximum, both the ZFC and FC magnetic susceptibilities show a Néel temperature bump

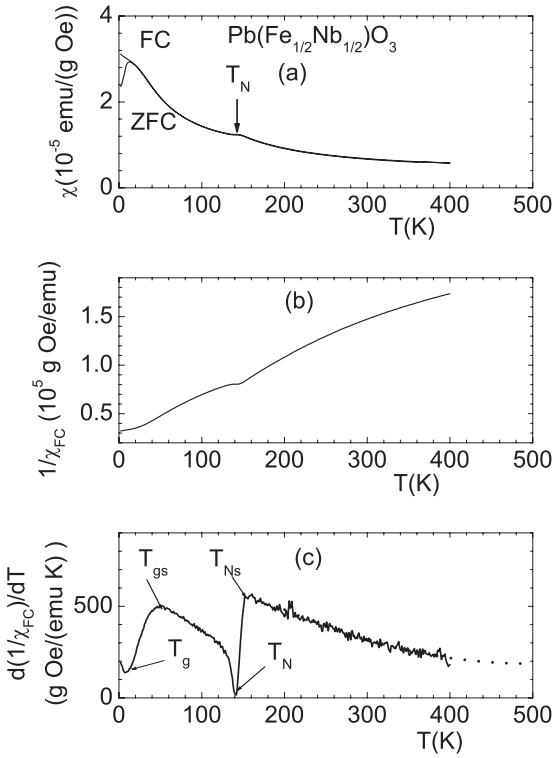

FIG. 1. (a) Temperature dependence of the ZFC and FC magnetic susceptibility of PFN measured in the applied field of 500 Oe. (b) Inverse of the susceptibility. (c) Derivative $d(1/\chi_{FC})/dT$ as a function of temperature. The dotted curve shows the extrapolation to $T = 500$ K.

at $T_N \approx 150$ K. This temperature is much lower than the temperature of the ferroelectric phase transition in PFN, which was found at ≈370–380 K.[4,6,7] It has been reported in Ref. 15 that the ferroelectric phase transition influences the magnetic susceptibility, and results in a magnetic anomaly at 370 K. We have not found such an influence in our measurements. Probably, this can be explained by the different origin of the samples used. For example, the powder sample used in Ref. 15 showed a weak ferromagnetism even at 370 K, while our single crystal sample was in the paramagnetic phase up to $T_N \approx$ 150 K.

Panels (b) and (c) in Fig. 1 present the inverse FC susceptibility $1/\chi_{FC}$ and derivative $d(1/\chi_{FC})/dT$, correspondingly. It can be seen that above T_N up to $T \approx 400$ K the derivative $d(1/\chi_{FC})/dT$ is not constant so that in this temperature region we cannot use the simple Curie-Weiss (CW) law $\chi = C/(T - \theta)$.

In order to estimate the magnetic moment per Fe^{3+}, we extrapolated the derivative $d(1/\chi_{FC})/dT$ towards higher temperatures, where it approaches a constant value [see the dotted curve in Fig. 1(c)]. In this way, we obtained the effective moment per Fe^{3+} equal to $\mu_{Fe} = 5.2\mu_B$. This value is not far from $5.4\mu_B$ reported by Bokov *et al.*[16] In the high-temperature region, we roughly estimated that the Curie-Weiss temperature was $\theta \approx -(450–500)$ K (comparable with $\theta = -520$ K estimated in Ref. 16).

Further, we can estimate the exchange constants using the following relations derived for a simple cubic lattice in the

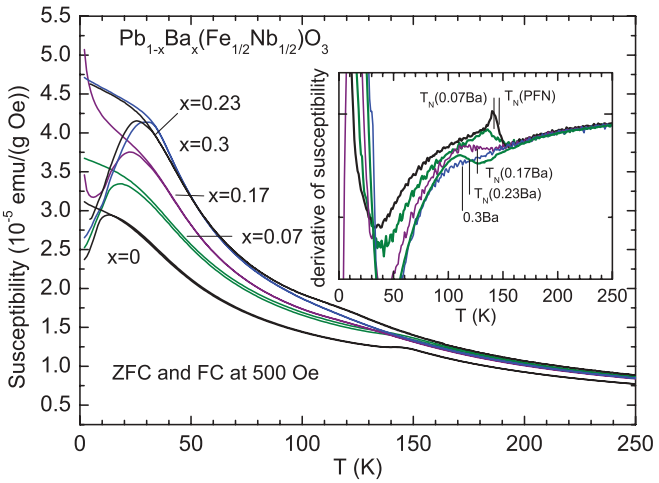

FIG. 2. (Color online) Temperature dependence of the magnetic susceptibility of $Pb_{1-x}Ba_x(Fe_{1/2}Nb_{1/2})O_3$, at $x = 0$, 0.07, 0.17, and 0.3, measured in the ZFC and FC modes, in a magnetic field of 500 Oe. The curves with a characteristic maximum at 13–30 K are ZFC data. To make the anomalies at temperatures of the AFM phase transition more visible, the inset shows the first derivative of the magnetic susceptibilities with respect to temperature.

molecular field approximation:[17]

$$T_N = \frac{2fS(S+1)}{3k}(-6J_1 + 12J_2),$$
$$\theta = \frac{2fS(S+1)}{3k}(6J_1 + 12J_2). \quad (1)$$

One can assume the common, for Fe^{3+}, spin value $S = 5/2$ and the $L = 0$ state; $f = 0.5$ is the average fraction of the Fe^{3+} ions assuming their random distribution over the B sites of the ABO_3 perovskite lattice, and J_1 and J_2 are the exchange constants of the nearest- and next-to-nearest-neighbor interactions, which correspond to the sites separated by the edge and face diagonals of the perovskite unit cell. By taking $\theta = -500$ K and $T_N = 150$ K, we have obtained $J_1/k = -19$ K and $J_2/k = -5$ K. These values are comparable with the data obtained earlier in the $LuFeO_3$ orthoferrite[18] ($J_1/k = -26$ K, $J_2/k = -4$ K) where a similar molecular field approximation was used. This simple analysis shows that the AFM phase transition in PFN is mainly determined by the nearest-neighbor interactions on the distance of the lattice constant a, such as $YFeO_3$ and $LuFeO_3$ orthoferrites. Such exchange interactions can exist in PFN only in the chemically disordered structure (see, e.g., Ref. 19). Obviously, in ordered PFN, only weak second-nearest- and fourth-nearest-neighbor interactions, $J_2 = J(a\sqrt{2})$ and $J_4 = J(2a)$, respectively, will exist. In this case, the magnetic phase transition would be shifted to lower temperatures and the long-range AFM order could even be suppressed.

The magnetic susceptibility data for the PFN-BFN single crystals are shown in Fig. 2. The compositions $x = 0$, 0.07, 0.17, and 0.23 show the bumps, in both the ZFC and FC susceptibility at 147, 145, 125, and 119 K, respectively. These bumps manifest an AFM phase transition characterized by the Néel temperature T_N. We found T_N to decrease, when the Ba concentration increases. However, simultaneously, the

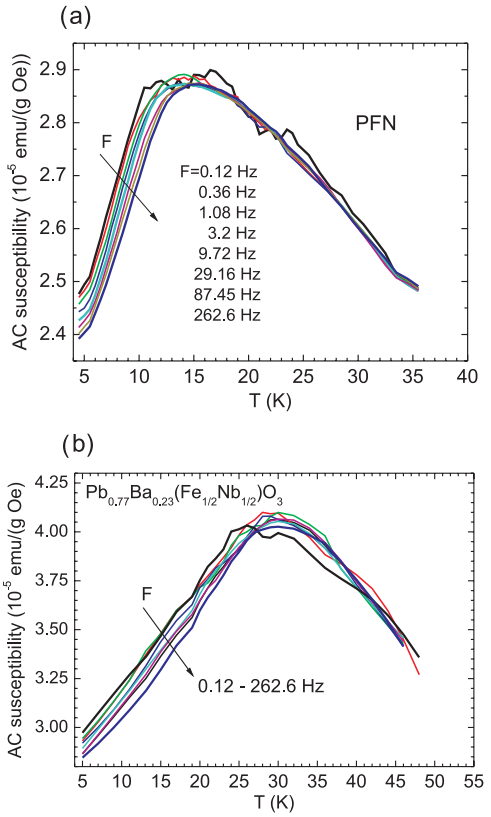

FIG. 3. (Color online) Temperature dependence of the ac magnetic susceptibility measured for (a) PFN and (b) $Pb_{0.77}Ba_{0.23}(Fe_{1/2}Nb_{1/2})O_3$ as a function of frequency at a field amplitude of 3.9 Oe.

susceptibility bump broadens, and becomes hardly visible, at a Ba concentration of $x = 0.3$. However, the first derivative of the magnetic susceptibility with respect to temperature still allows the observation of this diffused transition (see the inset in Fig. 2). In addition to a bump at the Néel temperature, we have clearly observed, for all Ba concentrations, a maximum of the magnetic susceptibility at lower temperatures. It shifts to higher temperatures with the increase of the Ba concentration, at least, up to $x = 0.3$, and essentially increases in magnitude. This low-temperature maximum is usually related to the spin-glass phase transition.[3,5] Note that, for all measured samples, there is irreversibility in the susceptibility measured in the ZFC and FC runs. This irreversibility is believed to indicate the presence of a spin-glass state characterized by a freezing temperature T_g, which is usually identified by the position of the temperature maximum of the ZFC susceptibility.[20]

The spin dynamics can be studied by means of the ac susceptibility measurements. Such data are presented in Fig. 3 for PFN and $Pb_{0.77}Ba_{0.23}(Fe_{1/2}Nb_{1/2})O_3$. The influence of the frequency can be characterized by a semiempirical factor:[21]

$$K = \Delta T_g/[T_g \Delta(\log F)], \quad (2)$$

which measures the frequency shift of T_g (defined here as the maximum of the real part of the ac susceptibility) per decade frequency F. Factor K yields the information if the system behaves as a classical spin glass or as a cluster glass (CG).[21] In PFN and 0.77 PFN-0.23 BFN, we obtained $K \approx 0.025$

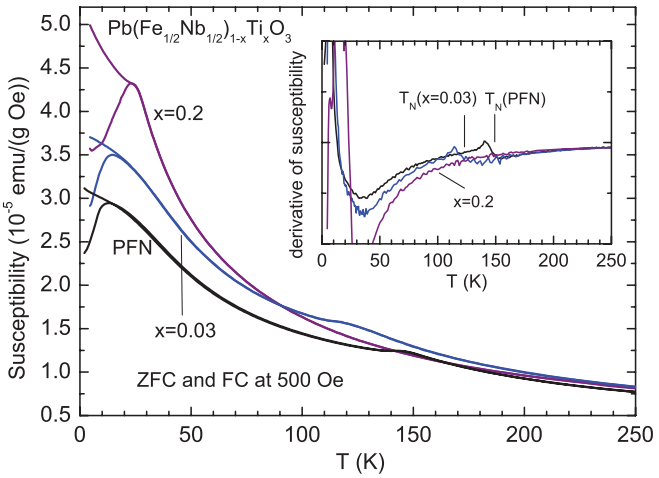

FIG. 4. (Color online) Temperature dependence of the magnetic susceptibility measured in ZFC and FC ($H = 500$ Oe) modes for PFN and $Pb(Fe_{1/2}Nb_{1/2})_{1-x}Ti_xO_3$ compositions at $x = 0.03$ and 0.2.

and 0.027, respectively, which corresponds to the CG case. For the classical SG systems, factor K is much smaller (e.g., $K \approx 0.005$ for CuMn).[21] These data confirm the fact that the Fe spins are strongly coupled in the glass phase of the solid solutions of PFN. Thus, further on, we will relate the low-temperature phase transition in $Pb_{1-x}Ba_x(Fe_{1/2}Nb_{1/2})O_3$ compositions to a CG phase transition, rather than to a SG one.

Figure 4 presents the temperature dependencies of the magnetic susceptibility obtained for $Pb(Fe_{1/2}Nb_{1/2})_{1-x}Ti_xO_3$ solid solutions in the ZFC and FC runs ($H = 500$ Oe). We found out that, at $x = 0.03$, there are two anomalies, one situated at 120–125 K and the other at 15 K. Since the behavior of $\chi(T)$ curves in Figs. 2 and 4 looks alike, we believe that these anomalies can be interpreted in a similar way. Specifically, the high-temperature anomaly stands for the Néel phase transition, whereas the low-temperature one refers to the SG or CG phase transition.

For the Ti content $x = 0.2$, the high-temperature bump is not visible due to significant smearing. Thus, the strong dilution of PFN with PT washes the AFM phase transition out. Notice that the low-temperature maximum is seen only in the ZFC run, but not in the FC one. Hence, the peak at 25 K most probably represents a SG or CG phase transition.

In order to prove the existence of the spin dynamics in PFN-PT we have measured the ac magnetic susceptibility for two PT concentrations, 0.03 and 0.2 (Fig. 5). It is seen, that the $\chi(T)$ plot shifts to lower temperatures, at low frequencies. This result is in line with our assumption about the SG or CG nature of the low-temperature phase transition at $T_g = 17.7$ K ($x = 0.03$) and $T_g = 25$ K ($x = 0.2$). In agreement with this idea, the susceptibility peak in $Pb(Fe_{1/2}Nb_{1/2})_{1-x}Ti_xO_3$ at $x = 0.2$ is sharp like in conventional SG.[21] We found the factor K for this composition to be smaller ($K \approx 0.01$) than the one for pure PFN or in PFN with a small amount of the Ti or Ba ions. The observed feature is typical of SG. Thus the strong dilution of PFN with $PbTiO_3$ transforms the CG low-temperature phase to a conventional SG one. This fact can be a result of the breaking of the Fe clusters down into smaller pieces, in such solid solutions.

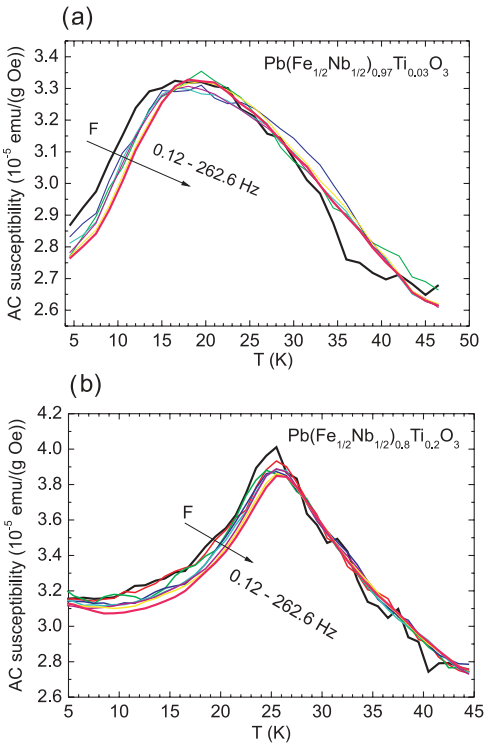

FIG. 5. (Color online) Temperature dependence of the ac magnetic susceptibility (given for several frequencies at the field magnitude of 3.9 Oe) for $Pb(Fe_{1/2}Nb_{1/2})_{1-x}Ti_xO_3$ solid solutions at (a) $x = 0.03$ and (b) $x = 0.2$.

B. Magnetization hysteresis loop studies

We have found that the hysteresis loops measured for PFN and its solid solutions at $T = 5$ K [see Figs. 6(a)–6(c)] are rather slim, which is inherent to spin glasses. However, we found that the remanent magnetization of the solid solutions is sufficiently larger than that for pure PFN. Thus, the doping was found to enhance the magnetic properties of PFN. This fact seems strange in light of the fact that the solid solutions under discussion have a smaller Fe or Pb content, which seems to facilitate the appearance of magnetism. Very probably, this evidence can be explained by the breaking of the large AFM clusters in the solid solutions of PFN into smaller and more disordered pieces possessing random and finite magnetic moments.

We also found out [see Fig. 6(d)] that the thermoremanent magnetization of $Pb(Fe_{1/2}Nb_{1/2})_{1-x}Ti_xO_3$ tends to vanish, on heating, toward 10, 13–15, and 25 K for $x = 0$, 0.03, and 0.2, respectively. These temperatures are close to the temperatures of the susceptibility maxima measured under the ZFC conditions. The essential increase of both the thermoremanent magnetization and magnetic susceptibility with Ti doping suggests that the net volume of the nonergodic SG or CG phase increases with Ti content. We observed a similar behavior in PFN-BFN solid solutions (not shown here). These facts, again, witness the breaking of the large AFM clusters in the solid solutions of PFN into smaller entities possessing finite (disordered) magnetic moments which can be assigned to a superparamagnetic, or more correctly, to superantiferromagnet clusters.[9] These clusters and their dynamics could also explain

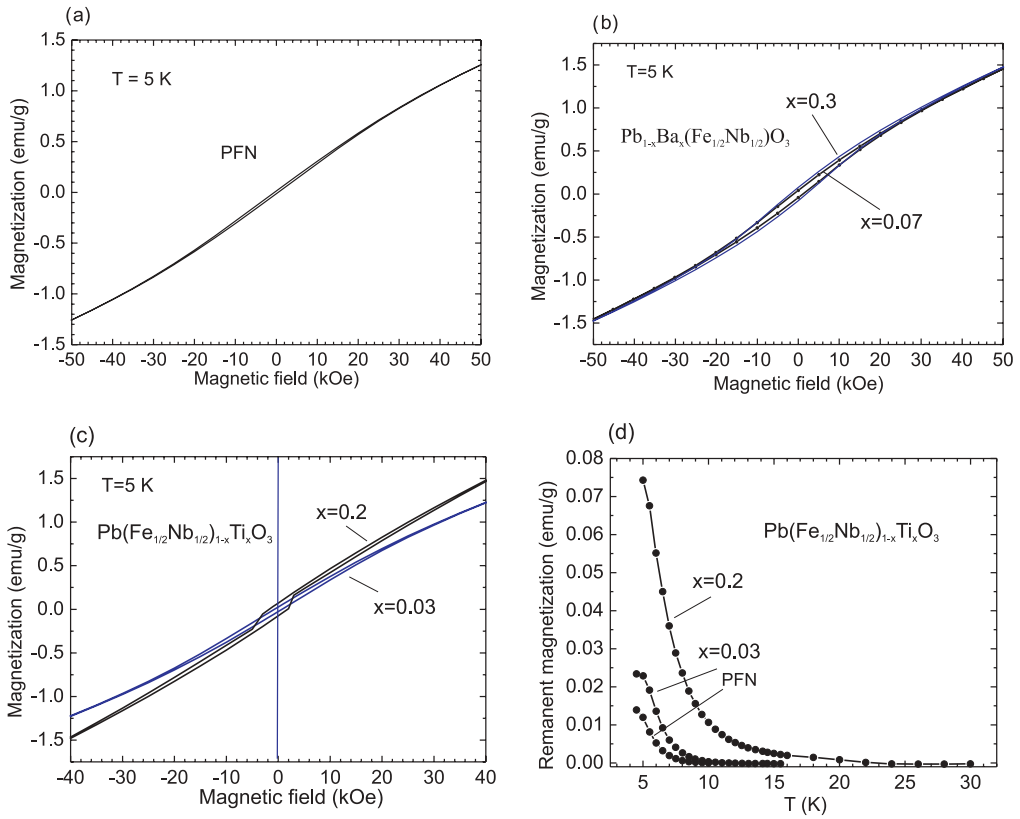

FIG. 6. (Color online) Magnetization hysteresis curves at $T = 5$ K [(a)–(c)] and temperature dependence of the thermoremanence (d) for PFN and some $Pb(Fe_{1/2}Nb_{1/2})_{1-x}Ti_xO_3$ and $Pb_{1-x}Ba_x(Fe_{1/2}Nb_{1/2})O_3$ compositions.

the monotonic increase of the susceptibility below T_N with decreasing temperature.

C. EPR data

We have measured the EPR spectra for different compositions of PFN-BFN and PFN-PT ceramics and single crystals, between 4 and 300 K. Most of the EPR measurements were performed using the ground into powder single crystals and ceramics, in order to minimize the influence of the conductivity and demagnetization fields on EPR line shape. Generally, we have not found a marked difference between the spectra measured from small crystals and their powders.

At room temperature, all samples studied showed the same one-line spectrum, which was attributed to the Fe^{3+} ions (Fig. 7).[10–13] We found the line shape to be Lorentzian or close to Lorentzian, with the peak-to-peak width at room temperature of about 60 mT for undoped PFN, in accord with earlier publications.[10,13] The small value of this width implies that the dipole-dipole linewidth and fine structure are narrowed by the exchange interaction. When temperature approaches the Néel temperature, on cooling, the linewidth critically broadens and the EPR line becomes invisible indicating the freezing of the spin fluctuations at EPR time scale.[22] This is illustrated by Fig. 7(a), where we present the evolution of the EPR spectrum of PFN with temperature decrease.

In contrast to this, in a $Pb_{1-x}Ba_x(Fe_{1/2}Nb_{1/2})O_3$ solid solution, the Fe^{3+} EPR spectrum only partly decreases in intensity at the Néel temperature as illustrated in Fig. 7(b) for the composition $x = 0.17$. However, at a lower temperature, T^*, the EPR spectrum disappears completely. The difference between the temperature, where the EPR spectrum disappears,

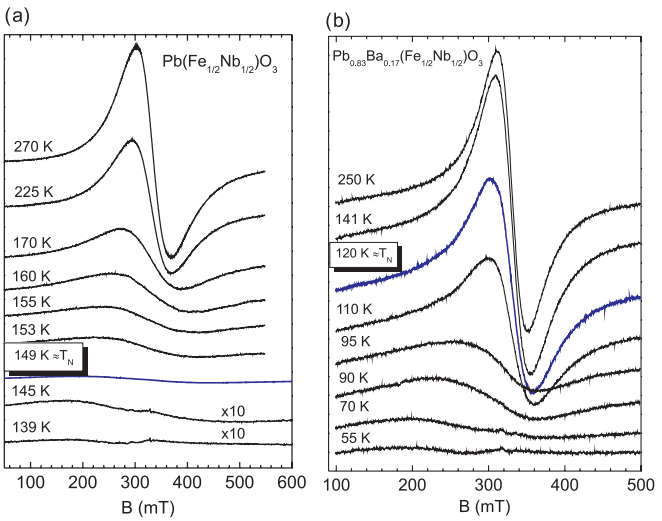

FIG. 7. (Color online) Temperature dependence of Fe^{3+} EPR spectrum in (a) PFN and (b) $Pb_{0.83}Ba_{0.17}(Fe_{1/2}Nb_{1/2})O_3$. With decreasing temperature the linewidth critically broadens and disappears in PFN at $T < T_N$. In $Pb_{0.83}Ba_{0.17}(Fe_{1/2}Nb_{1/2})O_3$, the Fe^{3+} spectral line does not completely disappear at $T < T_N$, indicating the coexistence of the AFM and paramagnetic phases up to about 60 K, on cooling.

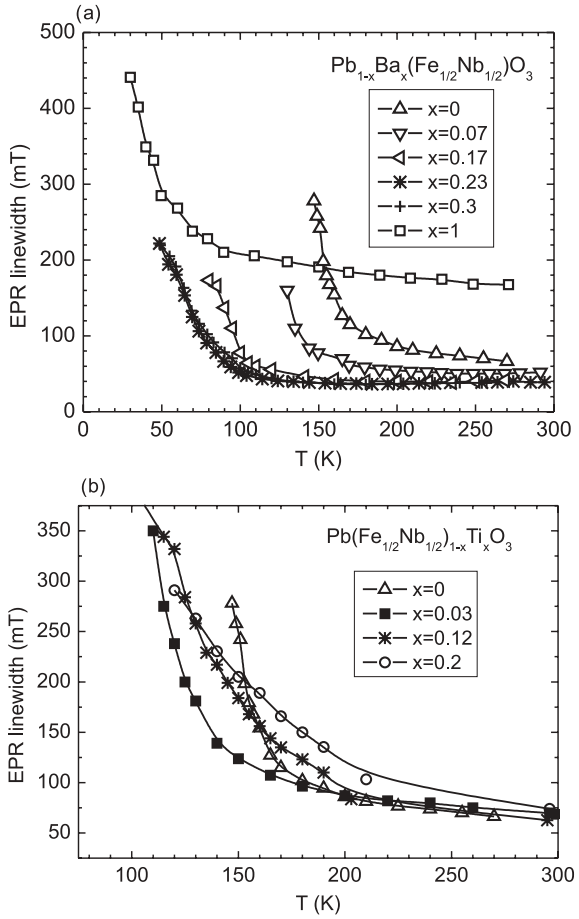

FIG. 8. Temperature dependence of the peak-to-peak EPR linewidth measured in the ground (a) $Pb_{1-x}Ba_x(Fe_{1/2}Nb_{1/2})O_3$ and (b) $Pb(Fe_{1/2}Nb_{1/2})_{1-x}Ti_xO_3$ single crystals and BFN ceramics ($x = 1$) showing the critical broadening when approaching the temperature of a magnetic phase transition.

and the Néel temperature, at $x = 0.23$, is 70 K [Fig. 8(a)]. This fact indicates that the long-range ordered AFM phase is created only in a part of the PFN-BFN crystals' volume, so that the rest of the volume remaining in the paramagnetic phase contributes to the EPR spectrum. With temperature lowering, the paramagnetic regions can gradually transform into the SAF phase leading to the broadening of the EPR spectrum and, finally, to its disappearance at T^*.

In $Pb(Fe_{1/2}Nb_{1/2})_{1-x}Ti_xO_3$ solid solutions, the situation is sharply different [Fig. 8(b)]. At low concentrations, below Ti content $x \approx 0.03$, the temperature T^* where the EPR signal disappears follows the trend of the Néel temperature, but, at higher concentrations, T^* becomes higher than T_N. Moreover, in a wide compositional range, T^* stays more or less constant, even for $x > 0.05$, where the AFM phase transition is not observed. We should note that, at large Ti concentrations, the linewidth almost smoothly increases with temperature lowering, and the critical broadening disappears. This indicates the change of type of the magnetic phase transition in PFN-PT due to the decrease of Fe concentration. In accord with the theory of EPR in AFM materials (see, e.g., Ref. 22), the broadening and disappearance of the EPR spectrum in the paramagnetic phase is related to the divergence of the decay rate of the magnetization fluctuations, when approaching the temperature of the magnetic ordering. In our case, the disappearance of the EPR spectrum in PFN-PT at $T^* = 110$–120 K may be interpreted as the appearance of an SAF phase.

IV. DISCUSSION

Let us now proceed with the consideration of possible physical models of the magnetic properties of PFN and its solid solutions with BFN and PT. We will discuss the cases of pure PFN and PFN-BFN and PFN-PT solid solutions separately.

A. PFN

Experimental data taken from literature and our data show that PFN experiences two different magnetic phase transitions on cooling. The former is related to the long-range AFM order, and the latter to the SG or CG phase. This sequence of the phase transitions has been explained by Kleemann *et al.*[3] We will employ this model, but we will reformulate it in terms of the percolation theory and in line with our experimental results. Imagine an infinite percolation AFM cluster, below the Néel temperature, made of a big part of the Fe disordered sites. However, not all the Fe sites contribute to this cluster, which is in accord with the theory of percolation.[23] The remaining part of the Fe sites organizes the so-called finite-size percolation clusters, which are structurally isolated from the infinite percolation cluster. The finite-size Fe percolation clusters are characterized not only by the local AFM moment, but also by a local FM moment. To illustrate this idea, consider, for example, a group of three structurally isolated nearest-neighbor Fe ions, in the sense that this group is surrounded by the Nb sites only. This nanoscale cluster cannot have a fully compensated magnetic moment, in a collinear consideration, because of the odd number of Fe ions, but it can have an AFM coupling of the nearest neighbors and a net FM moment. At T_N, the AFM moment can be essentially frozen, but the local magnetic moment in a given cluster may still frustrate contributing to the susceptibility. However, below T_g, these FM moments can freeze in, due to their coupling. In this case, if PFN is cooled under an external magnetic field, these FM moments can organize a FM ground state mixed with the AFM state of the main matrix. On ZFC, these clusters may freeze in the glass form. This picture has been established in Ref. 3 on the basis of the magnetic susceptibility measurements. By using our EPR data, we can be even more specific regarding the finite-size Fe clusters. We have found that the Fe^{3+} EPR signal is absent in PFN, below T_N. This striking fact implies that one should exclude from the finite-size Fe percolation clusters the independent and structurally isolated Fe^{3+} centers. Thus, with the precision of the EPR method, the minimal size of the Fe clusters includes more than one Fe site. We also emphasize that, in order to have the glass state, one has to take into account the coupling among such finite-size percolation clusters, and we believe that this coupling predominantly originates from the second-to-nearest-neighbor interactions, but the dipole-dipole interactions might be important as well.

In the discussion of the magnetic order in PFN we shall return to the derivative $d(1/\chi_{FC})/dT$ in Fig. 1(c). When

cooling PFN starting from high temperatures we saw a maximum in this derivative at $T = T_{Ns} \approx 156$ K, which is higher than the Néel temperature $T_N = 147$ K. Temperature T_{Ns} can be understood as the starting point of the development of the magnetic clusters. Above T_N, these clusters can be of a finite size, and long-range AFM order can be absent. On cooling, these clusters grow up, and at $T = T_N$, the infinite AFM percolation cluster shows up, for the first time. It is interesting that the derivative under discussion has a minimum at $T = T_N$, which can imply the loss of the spin dynamics, at this temperature. A similar situation occurs in the low-temperature region where a maximum in $d(1/\chi_{FC})/dT$ at $T = T_{gs} \approx 50$ K is followed by a minimum at 10 K. The latter temperature corresponds to the freezing temperature. Thus, temperature T_{gs} is the onset of the cluster growth, which finishes at T_g. It is worth mentioning that, in the same temperature interval, the diffuse neutron scattering intensity also grows up (Fig. 6 in Ref. 5).

B. PFN-BFN solid solutions

On the basis of the magnetic susceptibility and EPR data, we have constructed the phase diagram of PFN-BFN solid solutions which is shown in Fig. 9. The magnetic transition temperatures shown in Fig. 9 are assigned to anomalies in the ZFC magnetization measured under the field of 500 Oe. We observed the high-temperature bump in both the ZFC and FC susceptibility, up to $x = 0.23$. We found the Néel temperature to decrease linearly with increasing Ba concentration. The second, low-temperature ZFC susceptibility peak, associated with the spin-glass temperature T_g, shows a strongly nonlinear behavior with Ba concentration. At first, it slightly increases, but then saturates or even slightly decreases above $x \approx 0.2$–0.3. It is worth noting that a similar increase of T_g was observed previously in the PFN-PT solid solution ceramics in the $x < 0.1$ compositional range.[6] This increase was attributed to a slight decrease of the lattice parameter with x and a subsequent increase of the magnetic coupling. However, in the PFN-BFN system the lattice parameter increases with x[7] and such an explanation is not valid. We believe this increase of T_g to be a result of the increase of the average size of the confined percolation clusters, with Ba concentration, because of the decrease of the strength of the infinite cluster. Between T_N and T_g, the AFM phase coexists with the finite-size percolation clusters, which partly freeze below the spin-glass freezing temperature. For the BFN concentration larger than approximately $x = 0.3$, the PFN-BFN solid solutions seem to have only one, low-temperature phase transition, from the paramagnetic phase into a CG and/or SG phase. One can speculate that the long-range magnetic order does not exist at these concentrations. This assumption implies that the dilution of the Pb sublattice of PFN by Ba results in the breaking of the infinite magnetic percolation cluster responsible for the long-range AFM order and Néel temperature.

It is remarkable that, in PFN-BFN, the AFM phase splits into three different AFM phases (Fig. 9). One is below the line, at T^*, where the EPR spectrum disappears, and we attribute this phase to the mixture of the AFM and SAF phases. The second possibility can be found in between T^* and T_N. We attribute this phase to a mixture of the AFM and paramagnetic (PM) phases. Finally, there is also a supposed portion in the region, where the Néel temperature can disappear, but the SAF phase can still exist, together with the PM phase.

C. PFN-PT solid solutions

In PFN-PT solid solutions, the Néel temperature decreases with PT concentration much faster than in the case of PFN-BFN (Fig. 10). It is quite natural because the Fe content decreases in PFN-PT as x increases, while in PFN-BFN, the Fe content stays constant. Our experiment shows that the anomaly in the magnetic susceptibility corresponding to the AFM phase transition was not detected at $x > 0.04$. If one extrapolates the T_N vs x straight line, the critical composition for the disappearance of the AFM long-range order is expected to be at nearly $x \sim 0.1$. Below this concentration, the long-range

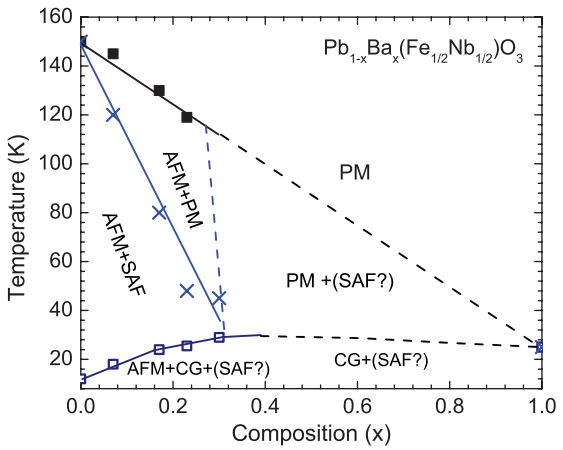

FIG. 9. (Color online) Phase diagrams of PFN-BFN. Filled squares correspond to the bumps, and empty squares to the peaks in the ZFC magnetization measured under the field of 500 Oe. Crosses show the temperatures T^*, where the EPR signal disappears. The solid and dashed lines separate different magnetic phases.

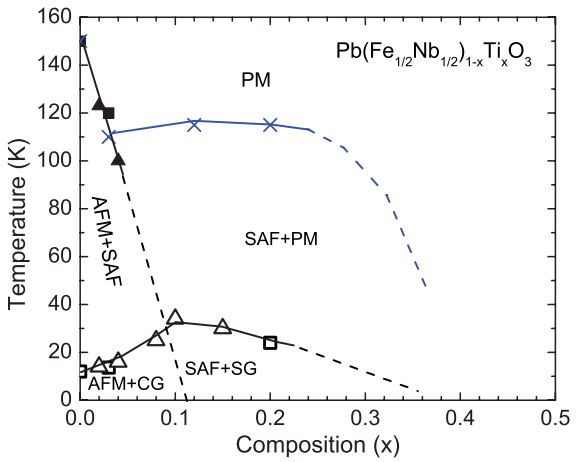

FIG. 10. (Color online) Phase diagrams of PFN-PT. Filled squares correspond to the bumps, and empty squares to the peaks in the ZFC magnetization measured under the field of 500 Oe. Crosses show the temperatures where the EPR signal disappears. The triangles are the data taken from Ref. 6. The solid and dashed lines separate different magnetic phases.

ordered AFM phase coexists with either the CG or the SG state, but, above, there can be only SAF and CG or SG phases.

As has been pointed out above, the EPR linewidth in PFN-PT solid solutions critically broadens and disappears when approaching temperature $T^* \approx 110$ K. This temperature is nearly constant in a wide concentration range, which manifests an interesting effect. EPR data suggest that below $T^* \approx 100$ K, SAF clusters grow up in the paramagnetic phase. This fact requires further studies and understanding. Another fact related to this finding can probably help in this understanding. We found that the magnetic susceptibility in PFN-PT is enhanced in the interval between T^* and T_g. This fact can be interpreted as the thermal fluctuations of the groups of the coupled spins having a net magnetic moment that is specific of relaxors.

V. SUMMARY

The results obtained clearly show that both *A*- and *B*-site dilutions of PFN result in the breaking of the infinite magnetic percolation cluster responsible for the long-range AFM order and Néel temperature. Under this doping, the long-range AFM state disappears and the SAF or SG or CG state becomes dominant. In the case of the PFN-PT solid solutions, such a consequence is natural, because of the decreasing Fe^{3+} content with x. However, the observation of these effects in the PFN-BFN solid solutions needs another explanation. We believe that the substitution of Pb by Ba has three possible consequences. First, this substitution changes the probability of the Fe clustering[19] and, correspondingly, changes the magnetic phase diagram. Second, this substitution introduces some disorder and structural changes, influencing the superexchange parameters, which control the AFM phase. Lastly, the third possibility is the straight influence of lead on the magnetic coupling between Fe^{3+} spins.[4]

We have found that the dilution of PFN with $PbTiO_3$ results in a percolation phase transition, at some finite concentration. Very probably, a similar phase transition also happens in PFN-BFN. As soon as such a (geometrical) phase transition is a critical phenomenon, one may expect an enhancement of all physical responses in the crystal matrix, and, in particular, the enhancement of the multiferroic response. This fact can be instructive in the search for good multiferroic materials.

The presence of the coexisting SG, CG, SAF, and AFM phases can be considered as the background for the "magnetic relaxor" features in the PFN crystal and its solid solutions, in analogy with ferroelectric relaxors.[24] We believe that the phase diagrams obtained for the PFN-based solid solutions will find their practical applications and will trigger new theoretical ideas.

ACKNOWLEDGMENTS

This study was supported by large infrastructure SAFMAT CZ.2.16/3.1.00/22132 and GACR 13-11473S projects, Ukranian SFFR (Contract No. F40/158-2012), and Russian Foundation for Basic Research (projects 11-02-90428_Ukr_f_a and 12-08-00887_a).

[1] A. Levstik, C. Filipič, and J. Holc, J. Appl. Phys. **103**, 066106 (2008).
[2] A. Levstik, V. Bobnar, C. Filipič, J. Holc, M. Kosec, R. Blinc, Z. Trontelj, and Z. Jagličić, Appl. Phys. Lett. **91**, 012905 (2007).
[3] W. Kleemann, V. V. Shvartsman, P. Borisov, and A. Kania, Phys. Rev. Lett. **105**, 257202 (2010).
[4] I. P. Raevski, S. P. Kubrin, S. I. Raevskaya, V. V. Titov, D. A. Sarychev, M. A. Malitskaya, I. N. Zakharchenko, and S. A. Prosandeev, Phys. Rev. B **80**, 024108 (2009).
[5] G. M. Rotaru, B. Roessli, A. Amato, S. N. Gvasaliya, C. Mudry, S. G. Lushnikov, and T. A. Shaplygina, Phys. Rev. B **79**, 184430 (2009).
[6] S. P. Singh, S. M. Yusuf, S. Yoon, S. Baik, N. Shin, and D. Pandey, Acta Mater. **58**, 5381 (2010).
[7] I. P. Raevski, S. P. Kubrin, S. I. Raevskaya, S. A. Prosandeev, M. A. Malitskaya, V. V. Titov, D. A. Sarychev, A. V. Blazhevich, and I. N. Zakharchenko, IEEE Trans. Ultrason. Ferroelectr. Freq. Control **59**, 1872 (2012).
[8] D. Varshney, R. N. P. Choudhary, C. Rinaldi, and R. S. Katiyar, Appl. Phys. A **89**, 793 (2007).
[9] L. Néel, J. Phys. Soc. Jpn. **17**, 676 (1962).
[10] A. Maryanowska and J. Pietzrak, Phys. Status Solidi A **68**, K185 (1981).
[11] G. Alvarez, R. Font, J. Portelles, R. Valenzuela, and R. Zamorano, Physica B **384**, 322 (2006).
[12] R. Blinc, V. V. Laguta, B. Zalar, B. Zupancic, and M. Itoh, J. Appl. Phys. **104**, 084105 (2008).
[13] V. V. Laguta, J. Rosa, L. Jastrabik, R. Blinc, P. Cevc, B. Zalar, M. Remskar, S. I. Raevskaya, and I. P. Raevski, Mater. Res. Bull. **45**, 1720 (2010).
[14] E. A. Dul'kin, I. P. Raevskii, and S. M. Emel'yanov, Phys. Solid State **39**, 316 (1997).
[15] R. Blinc, P. Cevc, A. Zorko, J. Holc, M. Kosec, Z. Trontelj, J. Pirnai, N. Dalai, V. Ramachandran, and J. Krrzystek, J. Appl. Phys. **101**, 033901 (2007).
[16] V. A. Bokov, I. E. Mylnikova, and G. A. Smolenskii, Sov. Phys. JETP **15**, 447 (1962).
[17] T. Nagamiya, K. Yoshida, and R. Kubo, Adv. Phys. **4**, 1 (1956).
[18] G. Gorodetsky, J. Chem. Solids **30**, 1745 (1969).
[19] I. P. Raevski, S. P. Kubrin, S. I. Raevskaya, D. A. Sarychev, S. A. Prosandeev, and M. A. Malitskaya, Phys. Rev. B **85**, 224412 (2012).
[20] A. Kumar, R. S. Katiyar, C. Rinaldi, S. G. Lushnikov, and T. A. Shaplygina, Appl. Phys. Lett. **93**, 232902 (2008).
[21] J. A. Mydosh, *Spin Glasses: An Experimental Introduction* (Taylor & Francis, London, 1993).
[22] D. L. Huber, Phys. Rev. B **6**, 3180 (1972).
[23] D. Stauffer, *Introduction to Percolation Theory* (Taylor & Francis, London, 1992).
[24] M. D. Glinchuk, Br. Ceram. Trans. **103**, 76 (2004).